

Analysis of Dam Break Wave Using Analytical, Computational Fluid Dynamics, and Experimental Approaches

Evi Noviani ^{a,*}, Yoga Satria Putra ^b, Cucu Suheri ^c

^a Department of Mathematics, Faculty of Mathematics and Natural Science, Tanjungpura University, Pontianak, West Kalimantan, Indonesia

^b Department of Physics, Faculty of Mathematics and Natural Science, Tanjungpura University, Pontianak, West Kalimantan, Indonesia

^c Department of Computer Systems Engineering, Faculty of Mathematics and Natural Science, Tanjungpura University, Pontianak, West Kalimantan, Indonesia

Corresponding author: *evi_noviani@math.untan.ac.id

Abstract—This research aims to examine the capability of the Computational Fluid Dynamics (CFD) method in simulating the behavior of dam break waves. It begins by building a 2D numerical simulation using OpenFOAM. To overcome the influence of turbulence, we employed the Large Eddy Simulation (LES) turbulent model, specifically the k-Equation and Smagorinsky model. The simulation was developed by applying the Navier-Stokes equations using the finite volume method in OpenFOAM. The analysis focuses on the free surface of a dam break. The results are in good accordance with both analytical and experimental results. The simulation has followed the trend of experimental and analytical free surface profiles at the dam break's early and late conditions. The low mesh number on the computational domain caused significant differences in the wavefront of the dam break. It reduced the accuracy of the calculation between the water and air interface. This study highlights the importance of understanding dam break wave behavior as part of risk mitigation for dam leakage. The behavior of dam break waves can be observed by determining observation positions at different locations, with the water gate of a dam serving as the reference point. These highly accurate numerical results indicate that the CFD approach employing OpenFOAM can be relatively cost-effective yet accurate in analyzing multiphase problems, such as dam breaks. This CFD approach is expected to contribute to developing mitigation and disaster prevention in the future.

Keywords— Computational fluid dynamics; dam break; OpenFOAM; turbulence model; large eddy simulation.

Manuscript received 26 Apr. 2023; revised 28 Aug. 2023; accepted 12 Sep. 2023. Date of publication 31 Dec. 2023.
IJASEIT is licensed under a Creative Commons Attribution-Share Alike 4.0 International License.



I. INTRODUCTION

Dams play a vital role in ensuring the availability of clean water, irrigation, power generation, and flood control for communities. They keep environmental stability and guarantee the quality of life for surrounding communities. However, in addition to a dam's inherent benefits, there are several risks associated with them, such as the potential damage (break) that might occur in the dam structure, commonly known as a dam break. A dam break can negatively impact the surrounding environment, such as agricultural land, infrastructure, and even people's lives. Some examples of DAM failures that have occurred in several countries include St. Francis Dam, the USA in 1928, Malpasset Arch Dam, France in 1959, Vajont Dam, Italy in 1963, Zhumadian Dam, China in 1975, Situ Gintung Dam, Indonesia in 2009, Way Ela Dam, Indonesia in 2013, and Kambaniru dam, Indonesia, in 2021 [1]–[6]. Therefore,

research analyzing dam breaks is still relevant today because these events have resulted in infrastructure damage and loss of life.

Based on the above reasons, conducting analytical, numerical, experimental, and on-site studies that examine dam break wave characteristics is essential. The study can help in disaster mitigation and emergency evacuation efforts, thus minimizing the number of casualties and infrastructure damage. It can also serve as a basis for academic studies on fluid physics and hydrodynamics. The research on dam break waves has been carried out for a long time [7]. Analytical and experiment studies, for example, were conducted to analyze the dam break wave propagation under different downstream conditions: dry and wet [8], [9]. These conditions lead to significantly different downstream flow patterns. In addition, the advancement of computational technology has made studies on dam breaks increasingly detailed and comprehensive. Numerical methods, including the CFD approach, have been repeatedly utilized to investigate the

physical characteristics of dam break waves [10]–[20]. The advantage of applying the CFD approach is that it can provide a detailed dam break wave's free surface profile compared to an analytical solution. Compared to the experimental method, the CFD approach has a higher efficiency at a lower cost [9], [21]–[23].

Previous research has contributed to completing studies related to dam breaks. Several CFD studies have compared the simulation results to analytical and experimental solutions [9], [24], [25]. A few researchers focused on studying the wave profile of a dam break. Several reports indicate that the application of the Reynolds-averaged Navier–Stokes (RANS) model with $k-\epsilon$ types, $k-\epsilon$ Renormalization-group (RNG), and $k-\omega$ has produced good results [26]. However, no one has reported the application of another turbulent model, namely the LES. The advantage of the LES model is that it can describe eddies in a fluid flow, which is essential in the case of a dam break where whirlpools can occur. Therefore, the objective of this study is to apply the LES model to investigate the free surface profile of a dam break and compare it to the analytical solutions proposed by [8] and the experimental results reported by [27], [28]. The dam break simulation was built using the CFD approach, applying the LES k -equation and Smagorinsky models [29]. This study will improve our understanding of water behavior during the event. Determining the scale and impact of the resulting disaster is crucial to assist us in mitigating the damage caused by a dam break.

II. MATERIALS AND METHOD

A. Numerical Domain

The first step of this study was constructing a 2D computational domain based on the experimental setup in two scientific works of literature, namely Kocaman (2007) and Khankandi (2012), as described in Figure 1 [27], [28]. The 2D simulation was constructed using the open-source software OpenFOAM, with dimensions adapted to match the experimental, as shown in Figure 1.

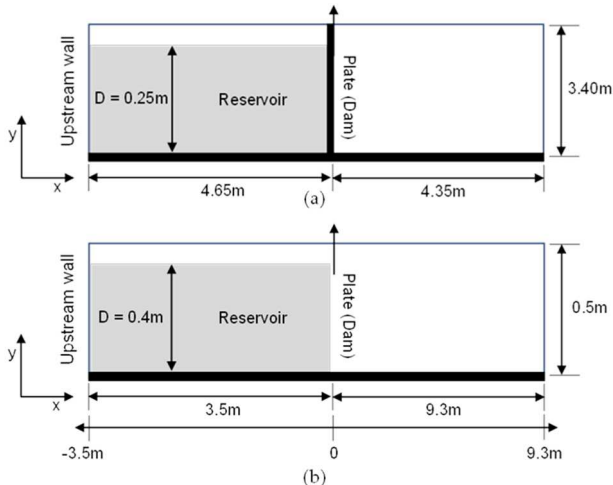


Fig. 1 Numerical domain in dam break simulation based on the experiment: (a) Kocaman [28], and (b) Khankandi [27]

The initial water depths in the two sketches were $D = 0.25$ m and 0.4 m, respectively. Figure 1(a) is used to analyze the behavior of the wave at the initial after the dam break occurs. The Kocaman experiment [28] provides information on the

characteristics of the wave early, which can be used as comparative data in this simulation. Meanwhile, Figure 1(b) analyzes the wave behavior when the dam break begins to recede. The Khankandi experiment [27] provides information on the shape of the free surface when the dam break wave recedes, which is then used for comparison in this simulation.

The dam break wave simulation in the horizontal plane has been generated using the open-source software OpenFOAM, applying the LES k -Equation and Smagorinsky turbulence models. To create geometries, we set all associated parameters in a file called *blockMeshDict*. The mesh/grid density of the domain was specified in this file, and we set the grid size to be $\Delta x \times \Delta y = (0.01 \times 0.01)m$, where Δx and Δy are the grid sizes on the x and y axes, respectively. In this file, we also determined the boundary conditions in the domain by applying the Dirichlet and Neumann boundary conditions. We generated the domain grids by executing the *blockMeshDict* file using the *blockMesh* command in the Ubuntu 22.04 LTS terminal. The initial water column conditions for the dam break case were set in an OpenFOAM library file named *setFieldsDict*. We generated the initial of the water column by executing the *setFieldsDict* file using the *setFields* command in the Ubuntu 22.04 LTS terminal.

B. Analytical Solutions

This study used the analytical solution for dam break waves in a horizontal bed with a wave tip region [28]. An analytical solution for an instantaneous free-surface profile has been generated for a horizontal channel, as shown in Figure 2.

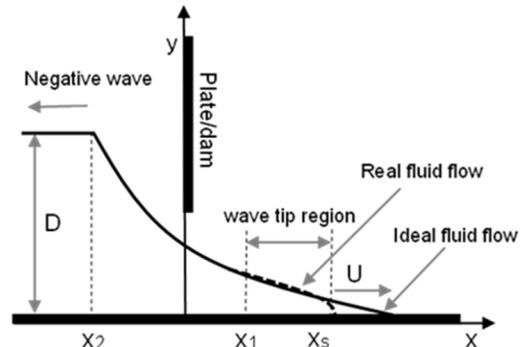


Fig. 2 Illustration of a dam break case as a basis for deriving an analytical solution with a wave tip region for a horizontal channel [8]

In this figure, the calculation domain is divided into four parts, namely $x \leq x_2$, $x_2 \leq x \leq x_1$, $x_1 \leq x \leq x_s$, and $x \geq x_s$ with initial water depth and the front wave celerity are D (m) and U (m/s), respectively. The Chanson analytic solution was obtained by deriving the Saint-Venant equation to define the dam break's free surface profile. Based on this Saint-Venant equation, Ritter (1892) derived analytical solutions for dam break problem with frictionless horizontal channels, which are expressed as follows [7]:

$$U = 2\sqrt{gd} \quad (1)$$

$$\frac{x}{t\sqrt{gD}} = 2 - 3\sqrt{\frac{d}{D}} \quad (2)$$

where U , d , D , x , t , and g are the front wave celerity, water depth, initial water depth, position with $x = 0$ at the dam,

time, and gravitational acceleration, respectively. Equations (1) and (2) give the wavefront velocity and the instantaneous profile at $t > 0$. From these Saint-Venant and Ritter solutions, Chanson obtains analytical solutions of the profiles on the four sections of the dam break wave, including the solution in the wave tip ($x_1 \leq x \leq x_s$) in laminar and turbulent flow [8].

In the current study, we gave the analytical solution for turbulent flow. This solution was chosen because the water flow was turbulent in the dam break case. In the horizontal conduit, the instantaneous profile of the dam break can be written as:

$$\frac{d}{D} = 1 \text{ at } x \leq x_2 \quad (3)$$

$$\frac{d}{D} = \frac{1}{9} \left(2 - \frac{x}{t\sqrt{gD}} \right)^2 \text{ at } x_2 \leq x \leq x_1 \quad (4)$$

$$\frac{d}{D} = \left(\frac{9}{32} G^{1/4} \left(\frac{U}{\sqrt{gD}} \right)^2 \frac{x_s - x}{D} \right)^{4/9} \text{ at } x_1 \leq x \leq x_s \quad (5)$$

(Wave tip region)

$$\frac{d}{D} = 0 \text{ at } x \geq x_s \quad (6)$$

where G is the dimensionless term defined as:

$$G = 3.65 \times 10^{-5} \frac{k_s}{D} + \frac{2.5 \times 10^{-3}}{Re_D \frac{U}{\sqrt{gD}}} \quad (7)$$

where k_s is the bed roughness thickness, and $Re_D = \rho \frac{\sqrt{gD^3}}{\mu}$ is the Reynolds number with the initial water depth D . The locations of x_1 , x_2 and x_s are determined respectively by the following equations:

$$\frac{x_1}{\sqrt{gDt}} = \left(\frac{3}{2} \frac{U}{\sqrt{gD}} - 1 \right) \quad (8)$$

$$\frac{x_2}{\sqrt{gDt}} = -1 \quad (9)$$

$$\frac{x_s}{D} = \left(\frac{3}{2} \frac{U}{\sqrt{gD}} - 1 \right) \sqrt{\frac{g}{D}} t + \frac{1}{6\alpha} \frac{Re_D}{\frac{U}{\sqrt{gD}}} \left(1 - \frac{1}{2} \frac{U}{\sqrt{gD}} \right)^6 \quad (10)$$

where α is a correction coefficient with $\alpha = 1$ for steady flow.

C. Numerical Method

This study utilized the OpenFOAM® v2206 software, primarily developed by OpenCFD Ltd. OpenFOAM®, a computational fluid dynamics software based on C++ language, to solve fluid mechanics-related problems. The water-air interface was described using The Volume of Fluid (VoF) method. This method uses volume fraction (γ) to define cells filled with different fluids with assumptions as in equation (11).

$$\begin{cases} \gamma(x, y, z, t) = 1 & (x, y, z), \text{ filled by water at time } t \\ 0 < \gamma(x, y, z, t) < 1 & (x, y, z) \text{ interface at time } t \\ \gamma(x, y, z, t) = 0 & (x, y, z), \text{ filled by air at time } t \end{cases} \quad (11)$$

To generate the dam break profile, OpenFOAM solves the advection equation using the MULES-VoF numerical scheme, which utilizes the Multidimensional Universal Limiter with Explicit Solution (MULES) in the *interFoam* solver [30]. The *interFoam* solver, which implements the capturing interface method, is used to solve multiphase problems. In the Volume of Fluid (VoF) method, the indicator function defined in equation (11) is solved in a transport

equation as in equation (12). The fluid phase fraction transport equation (Eqn. 12), the continuity equation (Eqn. 13), and the momentum equation (Eqn. 14) are solved simultaneously.

$$\frac{\partial \alpha}{\partial t} + \nabla \cdot (U\alpha) = 0 \quad (12)$$

$$\nabla \cdot U = 0 \quad (13)$$

$$\frac{\partial(\rho U)}{\partial t} + \nabla \cdot (\rho U U) = -\nabla p + \nabla \cdot T + \rho f_b \quad (14)$$

where γ , U , ρ , p , f_b are the fluid phase fraction, fluid velocity field, fluid density, pressure, and body forces per unit mass. Meanwhile, using an average rate of strain tensor $S = 0.5[\nabla U + (\nabla U)^T]$, and $I = \delta_{ij}$, we define T as a deviatoric viscous stress tensor: $T = 2\mu S - 2\mu(\nabla \cdot U)I/3$. In the VoF method, the force f_b includes gravity and surface tension.

The immiscible properties of the two fluids become an essential assumption in multiphase cases. The physical properties of the fluids are determined as the average values of the distribution of the volume fraction of each fluid. It means that the physical properties of each fluid are the same in the region it occupies, as shown in equations (15) and (16). It only varies around the interface.

$$\rho = \rho_w \gamma + \rho_a (1 - \gamma) \quad (15)$$

$$\mu = \mu_w \gamma + \mu_a (1 - \gamma) \quad (16)$$

where ρ_w , ρ_a , μ_w , and μ_a are the density of water, air density, water viscosity, and air viscosity, respectively. Furthermore, to determine the surface tension σ in the dam break wave, the form f_b in equation (14) is defined as

$$f_b = \sigma \kappa \nabla \gamma \quad (17)$$

with κ is the average curvature, which is calculated by the following equation:

$$\kappa = -\nabla \cdot \left(\frac{\nabla \gamma}{|\nabla \gamma|} \right) \quad (18)$$

Furthermore, to simplify the boundary conditions, the pressure in equation (14) is defined as:

$$p_d = p - \rho g \cdot \mathbf{x} \quad (19)$$

where \mathbf{x} is the vector of position. Equation (19) shows that the modified pressure p_d is the difference between the total pressure and the static pressure. By incorporating new definitions regarding dam break wave conditions, equation (14) can be written as:

$$\frac{\partial(\rho U)}{\partial t} + \nabla \cdot (\rho U U) - \nabla \cdot (\mu \nabla U) - (\nabla U) \cdot \nabla \gamma = -\nabla p_d - g \cdot \mathbf{x} \nabla \rho + \sigma \kappa \nabla \gamma \quad (20)$$

Furthermore, equations (12), (13), and (20) are solved using OpenFOAM by applying the finite volume method written in C++ to the *interFoam* solver.

D. LES Turbulent Model

In this study, the Smagorinsky model was used to overcome turbulence in the case of dam break waves. The LES model can be applied to resolve Navier-Stokes equations in large-scale flow cases employing the sub-grid scale (SGS) scheme. The filtered spatial velocity u in the LES model is expressed as:

$$u(x) = \int_{\Omega} u(x', t) G(x, x', \Delta) ds' \quad (21)$$

for a refined size Δ . In addition, we set $G(x, x', \Delta)$ as a spatial filter. Meanwhile, Ω is the domain. Spatial filters help adjust the grid size for large eddies and refine it for the small ones.

For the dam break case, the *tophat* G spatial filter was used with a definition like the following equation:

$$G = \begin{cases} 1/\Delta^3 & \text{if } |x-x'| \leq \Delta/2 \\ 0 & \text{otherwise} \end{cases} \quad (22)$$

where Δ is the filter size, i.e., $\Delta = (\Delta_1 \Delta_2 \Delta_3)^{1/3}$ with Δ_1 , Δ_2 , and Δ_3 are the width of the filter in partial coordinates. Furthermore, the velocity fluctuation in a flow is defined as:

$$\overline{u_i u_j} = \overline{u_i} \overline{u_j} + \overline{u_i' u_j'} = \overline{u_i} \overline{u_j} - \tau_{ij}^S \quad (23)$$

where τ_{ij}^S is the SGS stress tensor. Furthermore, the filtered Navier-Stokes equation can be expressed as:

$$\frac{\partial \overline{u_i}}{\partial t} + \overline{u_j} \frac{\partial \overline{u_i}}{\partial x_j} = -\frac{1}{\rho} \frac{\partial \overline{p}}{\partial x_i} + \frac{1}{\rho} \frac{\partial \overline{\tau_{ij}}}{\partial x_j} - \frac{\partial \tau_{ij}^S}{\partial x_j} \quad (24)$$

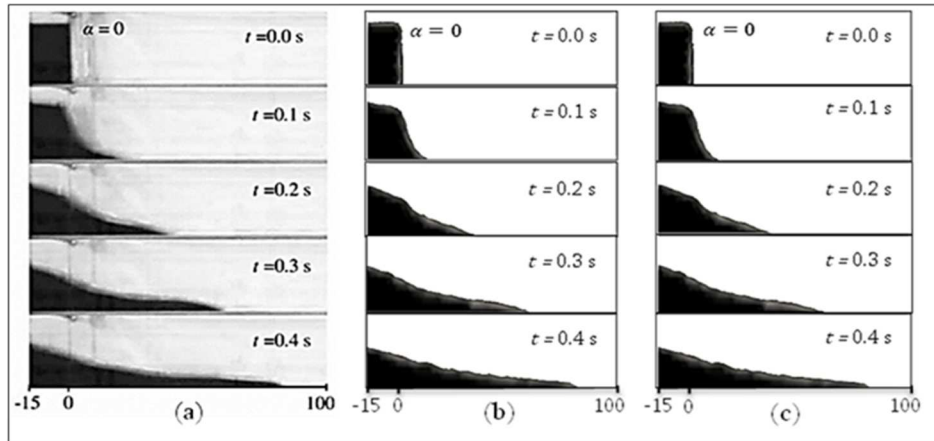


Fig. 3 Free surface evolution of dam break: (a) experiment [28]; numerically with turbulent models: (b) Large Eddy Simulation k-Equation, (c) Large Eddy Simulation Smagorinsky

This similarity confirms the applicability of the LES k-equation and Smagorinsky turbulence models for constructing dam break simulations. The qualitative comparison in Figure 3 can explain the mechanism of water movement after the dam break. When a dam break occurs, there are two paths of water movement: the positive path (to the right) and the negative (to the left). The initial depth decreases as the velocity of the dam break wavefront increases. In a dry-bed, water friction at the bottom of the canal can cause wavefront of the dam break to become convex [28]. The convex shape of the dam break wavefront has inspired an analytical solution, which is called the wave tip region (see equation (19)) [8]. However, Figure 3 only shows a qualitative comparison. Thus, a quantitative analysis must be carried out to make this comparative study of dam break wave cases provide complete information.

B. Free Surface in Early Condition

The profile in early conditions based on CFD numerical simulations is shown in Figure 1(a). The analysis related to the shape of the wave at the initial condition has been carried out by comparing the dam break profile of the CFD results with experimental [28] and analytical [8] results, as shown in Figure 4. The profile on the dry bed has been plotted based on the variation of dimensionless times $T = t(\frac{g}{D})^{1/2}$, where t , g ,

A. Free Surface Profile

This research successfully developed a dam break simulation with downstream dry-bed conditions using the CFD approach, specifically applying the LES k-equation and Smagorinsky turbulence models. Figure 3 shows a qualitative assessment of the dam break profile's shape from experimental results and the CFD simulation on a dry bed. The simulation results are displayed at different times: $t = 0$ s, 0.1 s, 0.2 s, 0.3 s, and 0.4 s. The comparison in Figure 3 demonstrates good agreement between the numerical calculations with OpenFOAM (Fig. 3(b), (c)) and the experimental results (Fig. 3(a)).

and D are the time (s), gravitational acceleration (m/s^2), and initial water depth (m), respectively. A quantitative comparison of the profile at the start of the dam break on a dry bed can be seen in Figure 4. We obtained four free surface profiles at six different time steps, $T = 0, 1.127, 2.755, 3.882, 5.009, \text{ and } 6.637$. The profiles were obtained from experimental, analytical, and numerical results and served as a validation of the CFD simulation results. An error analysis was carried out using the Root Mean Squared Error (RMSE) method to compare the numerical results with the experiments and the numerical results with the analytics. The RMSE values are described in Table 1.

The profile of the analytical results, which were obtained using equations (17), (18), (19), and (20), have been plotted successfully based on the physical conditions of the numerical simulation. The wave tip region's convex shape, modelled in equation (19), has also been successfully plotted, as depicted in Figure 4. Figure 4 (a) displays the initial of the profile for both numerical and analytical results since experimental data is unavailable. At this stage, the profile obtained by CFD simulation is identical to the analytic profile. However, differences appear at $T = 1.127$ (Fig. 4(b)) when the dam break occurs, and the numerical and experimental result profiles closely approximate each other.

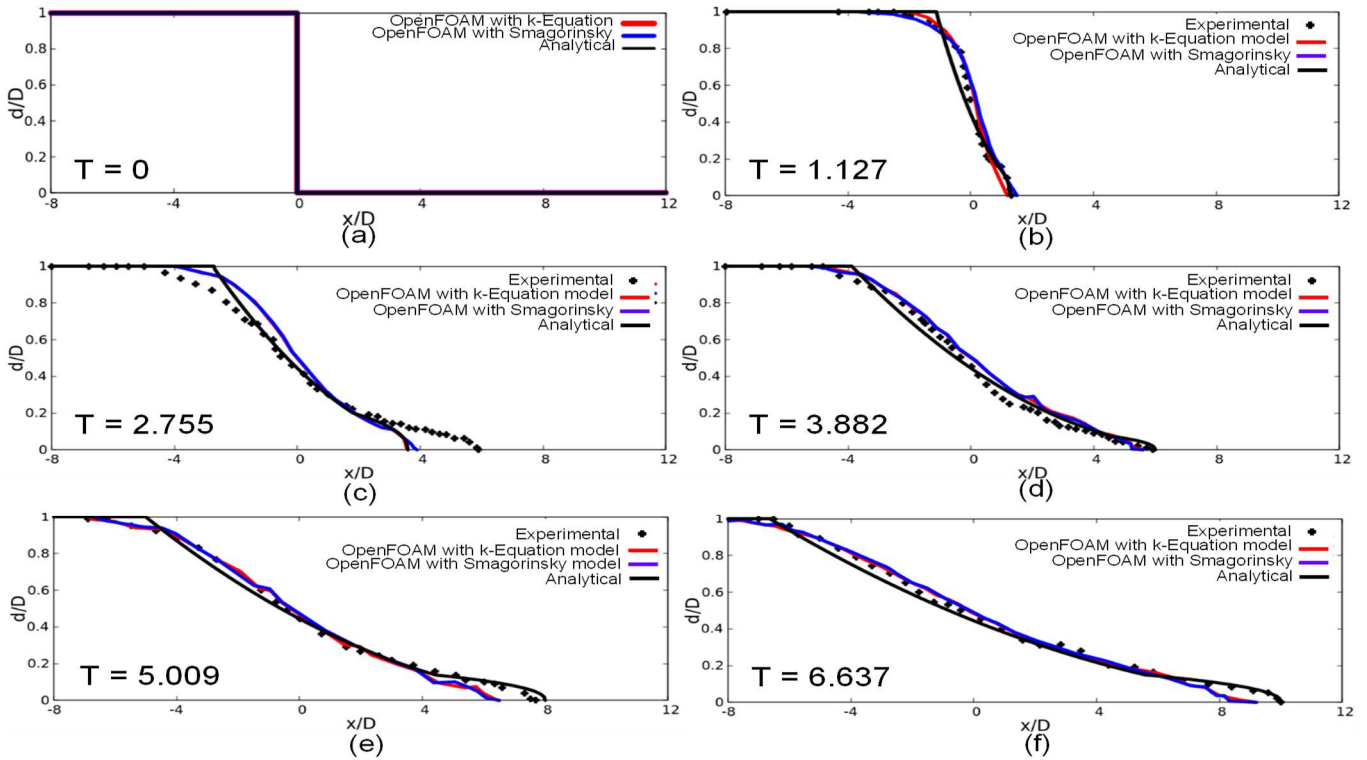


Fig. 4 The free surface dam break profiles from experimental results [28], analytical results [8] and numerical results using the LES k-Equation and Smagorinsky models at the initial dam break times with dimensionless times $T = t(\frac{g}{D})^{1/2}$ and dry-bed conditions ($\alpha=0$)

The assessment of the profiles between numerical, experimental, and analytical results is presented in Figure 4. The differences between these results are discussed, particularly in the wavefront profile of the dam break waves. The analytical curve slightly deviates from the numerical and experimental curves in the middle of the water column depth. Meanwhile, substantial differences occur in the frontal profile of the dam break waves. The CFD numerical wavefront profile is closer to the analytical profile in Figure 4(c) but drifts away from the experimental and analytical results in Figures 4(e) and (f). The inadequate density of meshes in the computational domain is believed to cause this significant difference. However, the small RMSE values in Table 1 suggest that the numerical solutions of the profiles have followed the trends of the experimental and analytical profiles.

TABLE I
THE RMSE VALUE FOR THE EARLY CONDITIONS OF THE DAM BREAK

Dimensionless Time (-)	RMSE			
	k-Eqn vs Exp	Smagorinsky vs Exp	k-Eqn vs Anal	Smagorinsky vs Anal
1.127	0,055	0,056	0,078	0,077
2.755	0,064	0,065	0,028	0,033
3.882	0,044	0,043	0,042	0,043
5.009	0,042	0,045	0,049	0,049
6.637	0,024	0,042	0,045	0,049

This result indicates that the LES k-Equation and Smagorinsky turbulence models effectively produce a free surface profile close to the experimental and analytical results. It should be noted that the k-Equation model has the smallest RMSE values among the Smagorinsky model.

C. Free Surface in Late Condition

The discussion on the dam break profile at the late condition is based on a CFD numerical simulation utilizing the computational domain, as depicted in Figure 1 (b). Applying the LES k-Equation and Smagorinsky turbulence models, a dam break simulation using the CFD approach has been developed. The profile of the numerical results is then plotted at the final times, $T = 9.899, 14.845,$ and 49.497 , after the dam break occurs, which is presumed to be the condition when the water begins to recede. Figure 5 displays an assessment of the profile generated from the experimental [27] and analytical results [8] with the results using the LES k-Equation and Smagorinsky models. The profiles generated from all three methods demonstrate excellent suitability for the late condition. The RMSE results show that the k-Equation model performs similarly to the Smagorinsky model, as presented in Table 2, with minimal RMSE values compared to experimental and analytical results.

TABLE II
THE RMSE VALUE FOR THE RECESSION OF WATER LEVEL

Dimensionless Time (-)	RMSE			
	k-Eqn vs Exp	Smagorinsky vs Exp	k-Eqn vs Anal	Smagorinsky vs Anal
9.899	0,009	0,009	0,011	0,019
14.845	0,016	0,016	0,005	0,007
49.497	0,007	0,007	0,003	0,003

The profiles generated from both numerical models agree perfectly with the analytical and experimental results. The reduction in the depth of the water column is depicted through the free surface profiles at three different times, indicating that the turbulence resulting from the friction of the water column

with a dry bottom is starting to disappear. As shown in Figure 5(c), the longer the dam break event occurs, the closer the formed free surface profile is to the horizontal line.

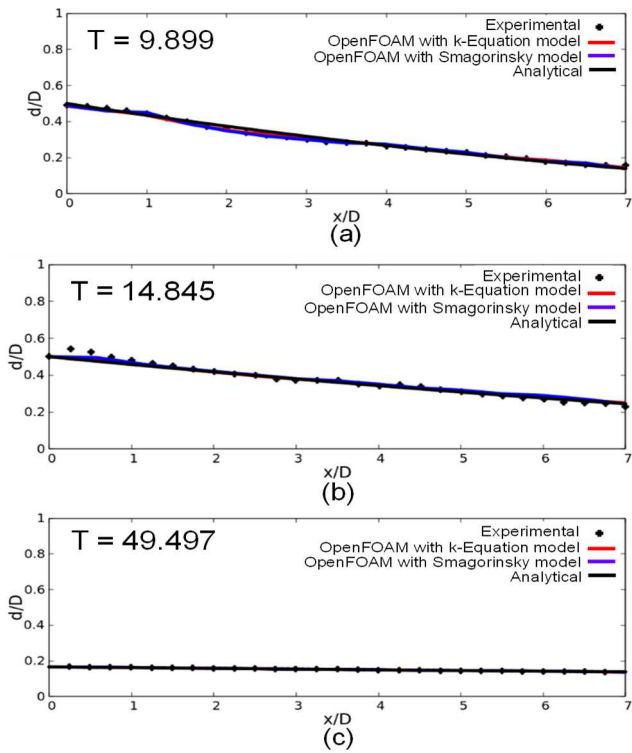


Fig. 5 Assessment of the dam break profile between experimental [27] and analytical results [8] with numerical results using the LES k-Equation and Smagorinsky at the late condition when the dam break wave begins to recede with dimensionless times $T = t(\frac{g}{D})^{1/2}$ and dry-bed ($\alpha = 0$)

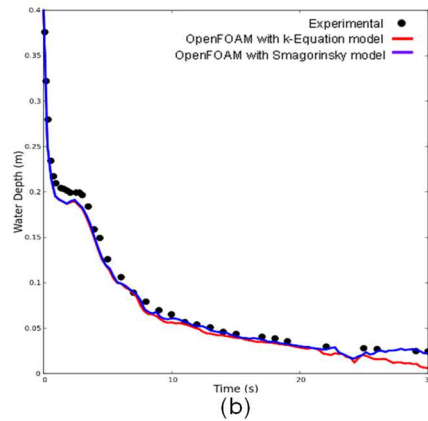
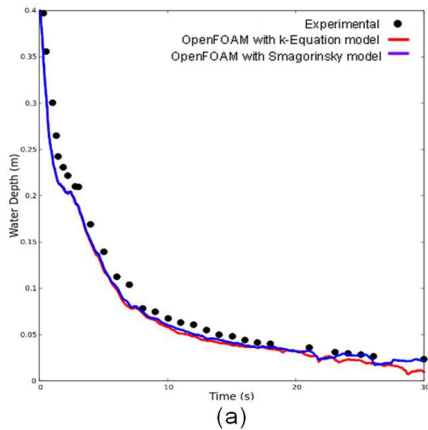
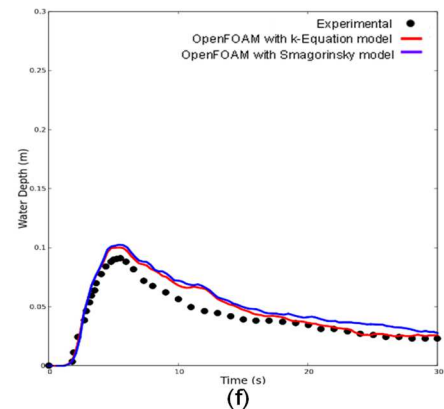
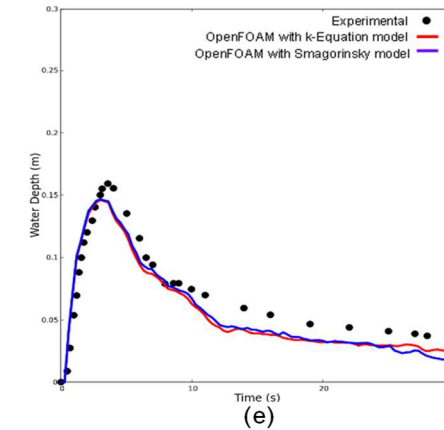
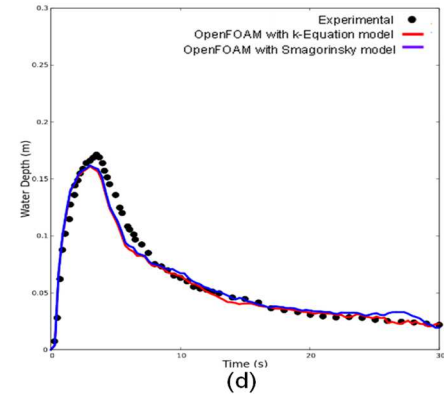
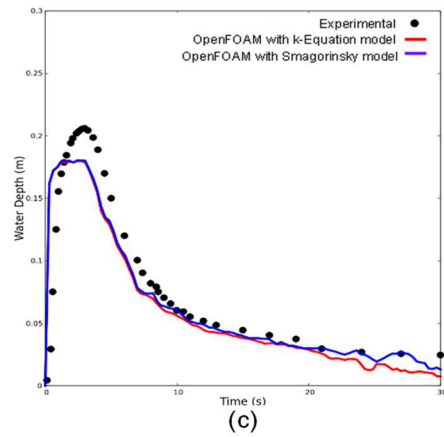


Fig. 6 Assessment of profile evolution from the simulation results with the LES k-Equation and Smagorinsky turbulence models to experiments [27] at six different x positions: (a) $x_1 = -0.5$ m; (b) $x_2 = -0.1$ m; (c) $x_3 = 0.1$ m; (d) $x_4 = 0.8$ m; (e) $x_5 = 1.2$ m; and (f) $x_6 = 5.5$ m

D. Profile Evolution of Dam Break

The final analysis conducted in this study involves an analysis of the shape of the dam break profile. The profile evolution analysis is concerned with fluctuations in the depth of the wave after the dam break occurs. Studying changes in depth during a dam break allows us to estimate the impact of the event, including its effect on water flow velocity, arrival time, and resulting wave height. Figure 6 illustrates the free surface evolution from simulation results using the k-Equation and Smagorinsky models with experimental results [27] at six different positions along the x -axis, namely $x_1 = -0.5$ m, $x_2 = -0.1$ m, $x_3 = 0.1$ m, $x_4 = 0.8$ m, $x_5 = 1.2$ m, and $x_6 = 5.5$ m. All correspond to the computational domain depicted in Figure 1(b). The free surface evolution depicted in Figure 6 begins with the initial conditions before the dam break, with an initial water level of $D = 0.4$ m and dry downstream conditions (dry-bed). The free surface evolution illustrated in Figure 6 was generated by integrating variables at six x positions using the free software Paraview version 5.8.0. The variations in water level at six x positions, both upstream and downstream of the sluice (located at $x = 0$ m), are depicted in Figure 6. The profile evolution at these six x positions exhibits satisfactory consistency with experimental [27] and numerical using the k-Equation and Smagorinsky models. This consistency is demonstrated quantitatively by the minimal RMSE values presented in Table 3, where the k-Equation model yields smaller RMSE values than the Smagorinsky model.

TABLE III
THE RMSE VALUE FOR FREE SURFACE EVOLUTION AT SEVERAL X POSITIONS

Position x (m)	RMSE	
	k-Eqn vs Experiment	Smagorinsky vs Experiment
-0.5	0,024	0,054
-0.1	0,011	0,007
0.1	0,015	0,022
0.8	0,009	0,009
1.2	0,016	0,016
5.5	0,006	0,014

The evolution at six positions along the dam break is presented by including positions $x_1 = -0.5$ m and $x_2 = -0.1$ m (upstream near the sluice gate), $x_3 = 0.1$ m, $x_4 = 0.8$ m, and $x_5 = 1.2$ m (downstream near the sluice gate), and $x_6 = 5.5$ m (far downstream). Due to the lack of available experimental data in this research, the evolution beyond x_6 could not be compared. Rapid changes in water depth were observed at x_1 and x_2 , where the initial water depth dropped from $D = 0.4$ m to $d = 0.02$ m within 30 seconds. The dam break wavefronts were detected downstream near the sluice gate at $x_3 = 0.1$ m, $x_4 = 0.8$ m, and $x_5 = 1.2$ m at times $t = 0.4$ s, 0.5 s, and 0.7 s, respectively. At $x_6 = 5.5$ m, the dam break wavefront appeared at $t = 2.0$ s. The maximum water depths downstream of the sluice gate (x_3 , x_4 , x_5 , and x_6) were recorded at $t = 3.0$ s, 3.5 s, 3.6 s, and 5.5 s, respectively, and decreased over time. The maximum water depth at each position was as follows: 0.206 m (x_3), 0.171 m (x_4), 0.159 m (x_5), and 0.091 m (x_6). This decrease in water depth is related to the reduction in potential energy, which can increase the kinetic energy on the wavefront. Therefore, further research is necessary to investigate the energy generated from dam break events.

IV. CONCLUSION

The comparative study of dam break waves was successfully conducted by developing a 2D numerical simulation using the CFD with the LES k-Equation and Smagorinsky models. The CFD simulation showed respectable qualitative and quantitative results with experimental and analytical results. The convex shape of the wavefront above the dry-bed was demonstrated through the analytical free surface curve, which was also in relatively good agreement with the free surface shape of the CFD numerical results.

The CFD numerical simulation utilizing the LES k-Equation and Smagorinsky models accurately replicated the free surface profile observed in the experimental and analytical data during the initial stages of the dam break. The simulation had a small RMSE value compared to experimental and analytical data, indicating its precision. Furthermore, the mesh number density influenced the dam break wavefront profile, as the computational domain was not densely meshed, leading to reduced accuracy in calculating the interface between water and air. While using the k-Equation and Smagorinsky LES turbulence models did not significantly impact the production of a free surface profile close to experimental and analytical results, the k-Equation model produced smaller RMSE values than the Smagorinsky model. When water receded in the final state, the CFD simulation produced the profile in agreement with the experimental and analytical results. The RMSE calculations revealed that the k-Equation and Smagorinsky models generated free surface dam break profiles similarly.

The free surface evolution of the dam break was analyzed at three horizontal positions - upstream near the sluice gate ($x_1 = -0.5$ m and $x_2 = -0.1$ m), downstream near the sluice gate ($x_3 = 0.1$ m, $x_4 = 0.8$ m, and $x_5 = 1.2$ m), and far from the sluice gate ($x_6 = 5.5$ m) using the k-Equation and Smagorinsky turbulence models. The numerical results show a good understanding of the experimental data at all three positions. The k-Equation model has a smaller RMSE value than the Smagorinsky model. The free surface evolution reveals that the initial depth of water changes rapidly at the upstream position near the sluice. The decrease in water depth at observation positions can be attributed to the decrease in potential energy. However, the decrease in potential energy can increase the kinetic energy on the dam break wavefront. Therefore, studies examining the energy generated from a dam break event can be interesting to pursue in the future.

NOMENCLATURE

CFD	Computational Fluid Dynamics
LES	Large Eddy Simulation
MULES	Multidimensional Universal Limiter with Explicit Solution
OpenFOAM	Open-source Field Operation and Manipulation
RMSE	Root Mean Squared Error
SGS	Sub-Grid Scale
VoF	Volume of Fluid

Greek letters

D initial water depth

m

d	water depth	m
G	spatial filter	
S	average rate of strain tensor	N/m^2
U	front wave celerity	m/s
Δx	mesh sizes at x axes	m
Δy	mesh sizes at y	m
γ	volume fraction	(-)
μ	Water viscosity	$Pa \cdot s$
ρ	Water density	kg/m^3
κ	average curvature	
Δ	filter size	

ACKNOWLEDGMENT

We sincerely thank the DIPA UNTAN grant for providing financial support for this research during the 2022 fiscal year. We thank the Faculty of Mathematics and Natural Sciences, Universitas Tanjungpura, for the resources and facilities used to conduct the computations for this research.

REFERENCES

- [1] H. Eldeeb, M. H. Mowafy, M. N. Salem, and A. Ibrahim, "Flood propagation modeling: Case study the Grand Ethiopian Renaissance dam failure," *Alexandria Engineering Journal*, vol. 71, pp. 227–237, May 2023, doi: 10.1016/j.aej.2023.03.054.
- [2] P. Paronuzzi, A. Bolla, D. Pinto, D. Lenaz, and M. Soccia, "The clays involved in the 1963 Vajont landslide: Genesis and geomechanical implications," *Eng Geol*, vol. 294, p. 106376, Dec. 2021, doi:10.1016/j.enggeo.2021.106376.
- [3] F. Aureli, A. Maranzoni, and G. Petaccia, "Review of Historical Dam-Break Events and Laboratory Tests on Real Topography for the Validation of Numerical Models," *Water (Basel)*, vol. 13, no. 14, p. 1968, Jul. 2021, doi: 10.3390/w13141968.
- [4] M. B. Adityawan *et al.*, "Numerical modeling of dam break induced flow through multiple buildings in an idealized city," *Results in Engineering*, vol. 18, p. 101060, Jun. 2023, doi: 10.1016/j.rineng.2023.101060.
- [5] E. M. Latrubesse, E. Park, K. Sieh, T. Dang, Y. N. Lin, and S.-H. Yun, "Dam failure and a catastrophic flood in the Mekong basin (Bolaven Plateau), southern Laos, 2018," *Geomorphology*, vol. 362, p. 107221, Aug. 2020, doi: 10.1016/j.geomorph.2020.107221.
- [6] I. Magdalena and M. F. Eka Pebriansyah, "Numerical treatment of finite difference method for solving dam break model on a wet-dry bed with an obstacle," *Results in Engineering*, vol. 14, p. 100382, Jun. 2022, doi: 10.1016/j.rineng.2022.100382.
- [7] A. Ritter, "Die Fortpflanzung der Wasserwellen," *Vereine Deutscher Ingenieure Zeitschrift*, vol. 36, no. 2, pp. 947–954, 1892.
- [8] H. Chanson, "Analytical solutions of laminar and turbulent dam break wave," in *River Flow 2006*, Taylor & Francis, 2006, doi:10.1201/9781439833865.ch48.
- [9] S. Oguzhan and A. O. Aksoy, "Experimental investigation of the effect of vegetation on dam break flood waves," *Journal of Hydrology and Hydromechanics*, vol. 68, no. 3, pp. 231–241, Sep. 2020, doi: 10.2478/johh-2020-0026.
- [10] R. Widiatmono, R. S. N. Mahmudah, I. Hidayat, K. A. Nugroho, and R. Y. Apriansari, "Investigation of Under-Relaxation Factors in 2D Dam Break Simulation of OpenFOAM®," *J Phys Conf Ser*, vol. 2377, no. 1, p. 012014, Nov. 2022, doi: 10.1088/1742-6596/2377/1/012014.
- [11] F. Garoosi, A. Nicole Mellado-Cusichua, M. Shademani, and A. Shakibaenia, "Experimental and numerical investigations of dam break flow over dry and wet beds," *Int J Mech Sci*, vol. 215, p. 106946, Feb. 2022, doi: 10.1016/j.ijmecsci.2021.106946.
- [12] Y. L. Li, C. P. Ma, X. H. Zhang, K. P. Wang, and D. P. Jiang, "Three-dimensional numerical simulation of violent free surface deformation based on a coupled level set and volume of fluid method," *Ocean Engineering*, vol. 210, p. 106794, Aug. 2020, doi:10.1016/j.oceaneng.2019.106794.
- [13] O. Simsek and H. Islek, "2D and 3D numerical simulations of dam-break flow problem with RANS, DES, and LES," *Ocean Engineering*, vol. 276, p. 114298, May 2023, doi: 10.1016/j.oceaneng.2023.114298.
- [14] W. Meng, C. Yu, J. Li, and R. An, "Three-dimensional simulation of silted-up dam-break flow striking a rigid structure," *Ocean Engineering*, vol. 261, p. 112042, Oct. 2022, doi:10.1016/j.oceaneng.2022.112042.
- [15] I. Magdalena, A. A. A. Hariz, M. Farid, and M. S. B. Kusuma, "Numerical studies using staggered finite volume for dam break flow with an obstacle through different geometries," *Results in Applied Mathematics*, vol. 12, p. 100193, Nov. 2021, doi:10.1016/j.rinam.2021.100193.
- [16] W. Liu, B. Wang, and Y. Guo, "Numerical study of the dam-break waves and Favre waves down sloped wet rigid-bed at laboratory scale," *J Hydrol (Amst)*, vol. 602, p. 126752, Nov. 2021, doi:10.1016/j.jhydrol.2021.126752.
- [17] A. Issakhov and A. Borsikbayeva, "The impact of a multilevel protection column on the propagation of a water wave and pressure distribution during a dam break: Numerical simulation," *J Hydrol (Amst)*, vol. 598, p. 126212, Jul. 2021, doi:10.1016/j.jhydrol.2021.126212.
- [18] D. H. Munoz and G. Constantinescu, "3-D dam break flow simulations in simplified and complex domains," *Adv Water Resour*, vol. 137, p. 103510, Mar. 2020, doi: 10.1016/j.advwatres.2020.103510.
- [19] A. Issakhov and Y. Zhandaulet, "Numerical study of dam break waves on movable beds for various forms of the obstacle by VOF method," *Ocean Engineering*, vol. 209, p. 107459, Aug. 2020, doi:10.1016/j.oceaneng.2020.107459.
- [20] A. Khoshkonesh, M. Daliri, K. Riaz, F. A. Dehrashid, F. Bahmanpouri, and S. Di Francesco, "Dam-break flow dynamics over a stepped channel with vegetation," *J Hydrol (Amst)*, vol. 613, p. 128395, Oct. 2022, doi: 10.1016/j.jhydrol.2022.128395.
- [21] T. R. Al-Husseini, A.-S. T. Al-Madhhachi, and Z. A. Naser, "Laboratory experiments and numerical model of local scour around submerged sharp crested weirs," *Journal of King Saud University - Engineering Sciences*, vol. 32, no. 3, pp. 167–176, Mar. 2020, doi:10.1016/j.jksues.2019.01.001.
- [22] D. G. Karkoulis, A. G. Panagiotopoulos, A. I. Giannaros, and D. P. Margaris, "A Comparison of Computational and Experimental Fluid Dynamics Studies between Scaled and Original Wing Sections, in Single-Phase and Two-Phase Flows, and Evaluation of the Suggested Method," *Computation*, vol. 10, no. 3, p. 33, Feb. 2022, doi:10.3390/computation10030033.
- [23] P.-E. Bournet and F. Rojano, "Advances of Computational Fluid Dynamics (CFD) applications in agricultural building modelling: Research, applications and challenges," *Comput Electron Agric*, vol. 201, p. 107277, Oct. 2022, doi: 10.1016/j.compag.2022.107277.
- [24] W. Liu, B. Wang, Y. Guo, J. Zhang, and Y. Chen, "Experimental investigation on the effects of bed slope and tailwater on dam-break flows," *J Hydrol (Amst)*, vol. 590, p. 125256, Nov. 2020, doi:10.1016/j.jhydrol.2020.125256.
- [25] L. E. Dumergue and S. Abadie, "Numerical study of the wave impacts generated in a wet dam break," *J Fluids Struct*, vol. 114, p. 103716, Oct. 2022, doi: 10.1016/j.jfluidstructs.2022.103716.
- [26] L. Peng, T. Zhang, Y. Rong, C. Hu, and P. Feng, "Numerical investigation of the impact of a dam-break induced flood on a structure," *Ocean Engineering*, vol. 223, p. 108669, Mar. 2021, doi: 10.1016/j.oceaneng.2021.108669.
- [27] A. F. Khankandi, A. Tahershamsi, and S. Soares-Frazaõ, "Experimental investigation of reservoir geometry effect on dam-break flow," *J Hydraul. Res*, vol. 50, pp. 376–387, 2012.
- [28] S. Kocaman, "Experimental and theoretical investigation of dam-break problem," Ph. D. Thesis, Civ. Engng. Dept, University of Cukurova, Adana, Turkey, Adana, Turkey, 2007.
- [29] OpenFOAM User Guide, "OpenFOAM The OpenFOAM Foundation User Guide," 2022. [Online]. Available: <https://openfoam.org>
- [30] J. R. K. Qvist and E. D. Christensen, "Development and implementation of a Direct Surface Description method for free surface flows in OpenFOAM," *Coastal Engineering*, vol. 179, p. 104227, Jan. 2023, doi: 10.1016/j.coastaleng.2022.104227.